Available online at www.sciencedirect.com
SCIENCE DIRECT
Talanta 68 (2006) 659–665
Talanta
www.elsevier.com/locate/talanta

Nanofluidic channels by anodic bonding of amorphous silicon to glass to study ion-accumulation and ion-depletion effect

Arindom Datta [a,*], Shubhra Gangopadhyay [a,1], Henryk Temkin [a], Qiaosheng Pu [b], Shaorong Liu [b]

[a] *Nano Tech Center, Texas Tech University, Lubbock, TX 79409, USA*
[b] *Department of Chemistry and Biochemistry, Texas Tech University, Lubbock, TX 79409, USA*

Received 3 January 2005; received in revised form 9 May 2005; accepted 10 May 2005
Available online 27 June 2005

Abstract

A unique phenomenon, ion-enrichment and ion-depletion effect, exists in nanofluidic channels and is observed in amorphous silicon (α-Si) nanochannels as shallow as 50 nm. As a voltage is applied across a nanochannel, ions are rapidly enriched at one end and depleted at the other end of the nanochannel. α-Si is deposited on glass by plasma enhanced chemical vapor deposition and is selectively etched to form nanochannels. The depth of nanochannels is defined by the thickness of the α-Si layer. Low temperature anodic bonding of α-Si to glass was used to seal the channel with a second glass wafer. The strength of the anodic bond was optimized by the introduction of a silicon nitride adhesion promoting layer and double-sided bonding resulting from the electric field reversal. Completed channels, 50 nm in depth, 5 micron wide, and 1 mm long were completely and reliably sealed. Structures based on nanochannels 50–300 nm deep were successfully incorporated into nanofluidic devices to investigate ionic accumulation and depletion effect due to overlapping of electric double layer.
© 2005 Elsevier B.V. All rights reserved.

Keywords: Ion-enrichment; Ion-depletion; Ion-accumulation; Nanochannels; Amorphous silicon

1. Introduction

Extremely small nanofluidic channels or structures are very important in research leading to detection and analysis of biomolecules like DNA and proteins at single molecule level [1–7]. Although some techniques are reported [1,6–8] to fabricate nanochannels for separation and analysis of biomolecules, there is still a need for a simple and reliable microfabrication technique to make nanosized channels. The challenge is to fabricate such structures or systems with existing processing techniques. In this paper, we report the observation of the ion-enrichment and ion-depletion effects inherent with nanochannel structures and a simple but efficient method to fabricate these nanochannels using a combination of conventional microfabrication techniques with anodic bonding. Nanochannels are formed in α-Si deposited on glass substrates by plasma enhanced chemical vapor deposition (PECVD) and patterned precisely by reactive ion etching. The depth of the channel is strictly defined by the thickness of the α-Si layer. The channels are sealed by anodic bonding with a second glass substrate. In this connection, anodic bonding between α-Si (deposited by PECVD) and glass was studied in some detail. A similar technique to fabricate nanochannels, however, is reported [9] very recently, but they used LPCVD α-Si as an intermediate layer and different dry etch chemistry than ours to etch little deeper into glass. Since there is significant difference in properties between PECVD and LPCVD silicon nitride, it is also of importance to study nanochannels in amorphous silicon film deposited by PECVD.

Anodic bonding was introduced by Wallis and Pomerantz [10] as a technique for joining metal to sodium containing glass. Since then it has also been used intensively

* Corresponding author. Present address: University of Wisconsin-Madison, Department of Mechanical Engineering, 1513 University Ave., Madison, WI 53706, USA. Tel.: +1 608 262 3490; fax: +1 608 265 2316.
E-mail address: adatta@cae.wisc.edu (A. Datta).
[1] Present address: University of Missouri-Columbia, Columbia, MO 65211, USA.

0039-9140/$ – see front matter © 2005 Elsevier B.V. All rights reserved.
doi:10.1016/j.talanta.2005.05.011

for silicon-to-glass bonding, and it is a useful technique in micromechanics, for cavity sealing, device encapsulation [11–13]. The metal, or semiconductor, is bonded to the glass by applying an external voltage with simultaneous heating, at temperatures compatible with microelectronic processing. The cathode makes contact with the glass, and metal, or semiconductor, is the anode. At the bonding temperature, the Na^+ ions coming from the dissociation of NaO_2, are mobile, and migrate towards the cathode, leaving behind the oxygen ions. A negatively charged depletion layer is thus formed adjacent to the anode. The electrostatic force between this negative layer and the positive charge induced on the anode brings the two sides into intimate contact. In case of Si, it is believed that O_2 ions leave the glass due to the high electric field and form Si–O–Si bonds, i.e. a thin SiO_2 layer is formed. This assumption is supported by observation of a thin SiO_2 layer by Rutherford back scattering (RBS) [14].

In the bonding process, external voltage is applied between the heating plate (anode) beneath the Si and a point contact (cathode) on the glass. The bonding starts at the point contact and spreads radially. The radially spreading bonding front makes it less likely for air to become trapped between the Si and the glass. Borosilicate glass (e.g. Corning Pyrex 7740 glass) is usually used since it has a thermal expansion coefficient that is almost equal to that of Si. It also has the necessary electrical conductivity at the temperature at which the bonding process takes place. Pyrex glass consists of 80% SiO_2, 13% B_2O_3, 3.5% Na_2O, and 2.35% Fe_2O_3 and Al_2O_3. Although soda lime glass has more sodium than Pyrex, it is very difficult to use in anodic bonding because of large mismatch of thermal expansion coefficients.

The strength of bonding between the two wafers sealing channels is very important for performance of micro/nanofluidic devices. Abe et al. [15] gave detailed account on bond strength between thermally attached quartz and thinned Si wafer. They observed a relationship between the thickness of Si and the bonding temperature required for complete bonding to take place. Maszara et al. [16] measured the bond strength of thermally bonded oxidized Si wafers. In crack propagation experiments, the surface energy was found to increase with the bonding temperature. Obermeier [17] reported on Si to Pyrex bond strength measurements. However, in all samples the break occurred in the glass and not at the Si/glass interface and the bond strength could not be determined. Although there are some reports available [18–20] for glass to glass bonding using an intermediate thin amorphous silicon layer (not deposited by PECVD), little is known about the bond strength of PECVD amorphous Si to glass system. Choi et al. [18] studied glass-to-glass electrostatic bonding for providing an in situ vacuum packaging of an FED panel in an ultra-high-vacuum chamber using amorphous silicon films deposited by radiofrequency (rf) sputtering technique on Sn-doped In_2O_3 coated glass substrates. Berthold et al. [19] studied glass to glass anodic bonding using standard IC technology thin films including LPCVD polysilicon and amorphous silicon as intermediate layer. Recently, Wei et al. [20] reported an increase in bond strength if a hydrogen free amorphous silicon layer is sputter deposited on silicon substrate before bonding it to a glass wafer.

In our investigation, we studied the bond strength between PECVD α-Si coated borofloat glass and bare borofloat glass wafers. The goal was to produce sealed structures, allowing us to study the behavior of fluids in nanometer-scale channels which is not expected to be same in channels of micron depth.

The present study, thus, includes the preparation of nanochannels and the demonstration of the ion accumulation and depletion effects as ionic species are electrophoretically transported through these channels. These effects are caused by the overlapping electric double layer, inherent to nanochannels.

2. Experimental

2.1. Anodic bonding

The process was carried out on temperature controlled heater plate capable of reaching 500 °C. A dc power supply was connected to bias the α-Si positively with respect to glass (Fig. 1). A current meter was connected in series to measure the time evolution of current during bonding and to monitor the progression of bonding. A typical bonding process was carried out on wafers 100 mm in diameter, at 350–400 °C, and a bias of 1–1.2 kV for 20 min. The current behavior during bonding of glass to α-Si is illustrated in Fig. 2. The initial current increased rapidly to as high as ∼7 mA and decayed to the level of ∼2 mA in about 3 min time. Further decrease in current occurred very slowly. The bonding takes place in the initial 3–4 min but the bond gets stronger as the wafers are kept for longer time under electric field.

2.2. Deposition of amorphous silicon and dry etching

Thin films of amorphous silicon (α-Si) with different thicknesses were deposited in a P-5000 cluster tool (Applied Materials) at a susceptor temperature of 350 °C and a chamber pressure of 2.5 Torr. The plasma power was maintained at 50 W and gas flows of 200 sccm SiH_4 in 2000 sccm Ar were used. Under these conditions, layers of α-Si with the thickness range of 50 nm to 1.5 μm could be readily deposited at a rate of ∼180 nm/min. A thin layer of silicon nitride was

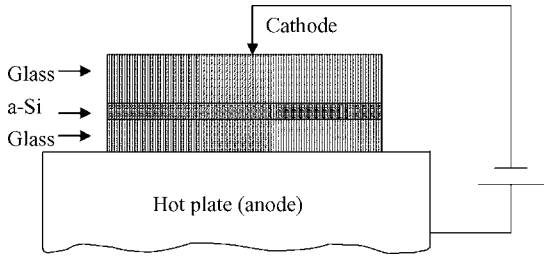

Fig. 1. Schematic of anodic bonding setup.

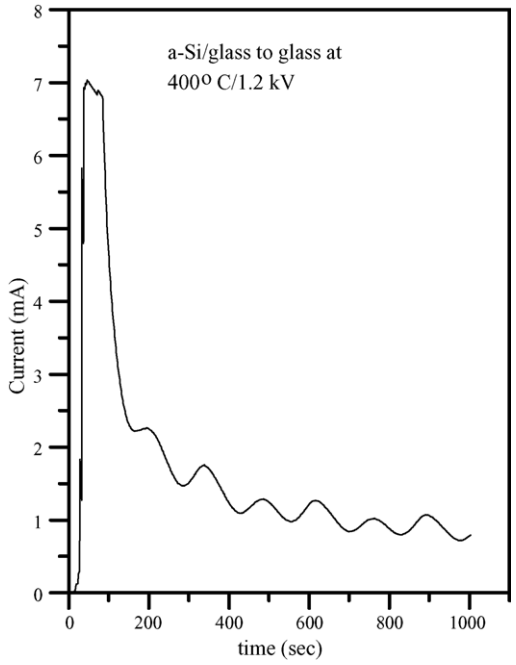

Fig. 2. Behavior of current as a function of time during anodic bonding.

deposited, in some wafers, between the glass substrate and the α-Si. Its purpose was to improve adhesion between α-Si and the glass and thus produce a stronger bond in the subsequent nanofluidic device. The 8 nm thick adhesion layer of Si_xN_y was also deposited at 350 °C, a chamber pressure of 4 Torr. The layer was prepared using gas flows of 25 sccm of SiH_4, 1500 sccm of N_2, and 1000 sccm of Ar, at a plasma power of 100 W. Prior to deposition borofloat glass substrates were degreased in acetone, methanol, and de-ionized (DI) water followed by Piranha etch (H_2SO_4:H_2O_2 = 2:1) and a second DI water rinse.

The channel structure was defined by photolithography and the exposed α-Si was dry etched in an inductively coupled plasma (ICP) chamber. We used C_2F_6 at 80 sccm and O_2 at 7 sccm, resulting in the chamber pressure of 160 mTorr, under ICP power of 300 W. These conditions resulted in an etch rate of ∼75 nm/min.

2.3. Fabrication of nanochannels and anodic bonding

Two lithographic masks, one containing an array of nanochannels of varying widths and lengths (Mask-I) and another containing U-shaped microchannels for connecting the nanochannels at both ends (Mask-II), were used. The nanochannels were prepared in α-Si layers of varying thickness used as spacers between two glass wafers, with the thickness of the α-Si layer defining the channel depth. The channel width was defined lithographically using Mask-I and the channel array transferred into the α-Si layer by dry etching. Another glass substrate was covered with a relatively thick layer of α-Si (∼600 nm) and patterned with Mask-II forming microchannels. On this wafer, the microchannels were plasma etched into the α-Si and the glass was patterned using wet etching in HF (48 wt%) for 5 min to form channels ∼50 μm deep. Access holes, 1 mm in diameter, were drilled at the termination of the U-shaped microchannels using diamond bits. The photoresist was subsequently removed from both wafers in acetone under ultrasonic agitation and α-Si was removed from the wafer with glass channels using KOH. The two wafers were then aligned under a microscope and anodically bonded to fabricate complete devices. We have successfully fabricated nanochannels with the depth of 50 nm, 100 nm, 220 nm, 300 nm, 922 nm, and 1475 nm using this process. It is important to point out that the low temperature of bonding, ∼400 °C, allows us to prepare very shallow nanochannels with high degree of precision. The bonding temperature is well below that of the softening point of glass, 620 °C, and the channels are not deformed in the bonding process. In all devices, plastic ports used as reservoirs were attached with epoxy to facilitate injection of fluids into nanochannels. A photograph of a typical device is shown in Fig. 3.

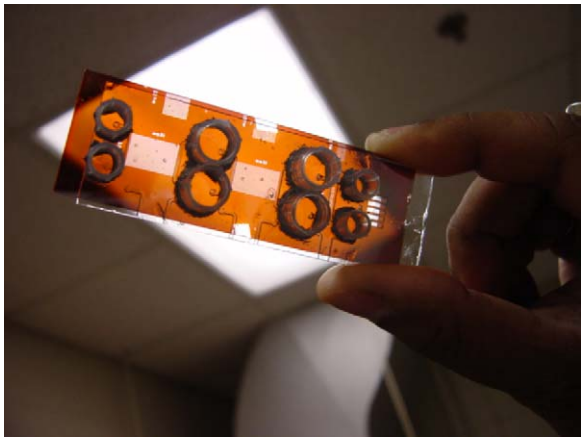

Fig. 3. A complete device with ports attached.

2.4. Bond strength measurements

Bond strength was measured using an Instron tensile tester with different sample configurations. For shear test, two glass slides (each 1 mm thick) were used and an area of quarter by 1 in. (1/4 in. × 1 in.) was bonded. Aluminum (Al) strips, 1–2 mm thick, were glued to the unbonded glass surfaces to give extra strength and support to the sample. It is to be noted that glass is brittle and samples break in the shear test even after taking this precaution. A less damaging pull test was also used. Test structures, 5 mm × 5 mm areas of α-Si defined on a glass wafer by patterning and dry etching in a 25 mm × 25 mm sample, were prepared for this experiment. Such structures were then anodically bonded to bare glass wafers of same size and tested. A special jig was made and glued to one side of the sample and an Al strip was glued to the other side. Fig. 4(a and b) shows the test configuration.

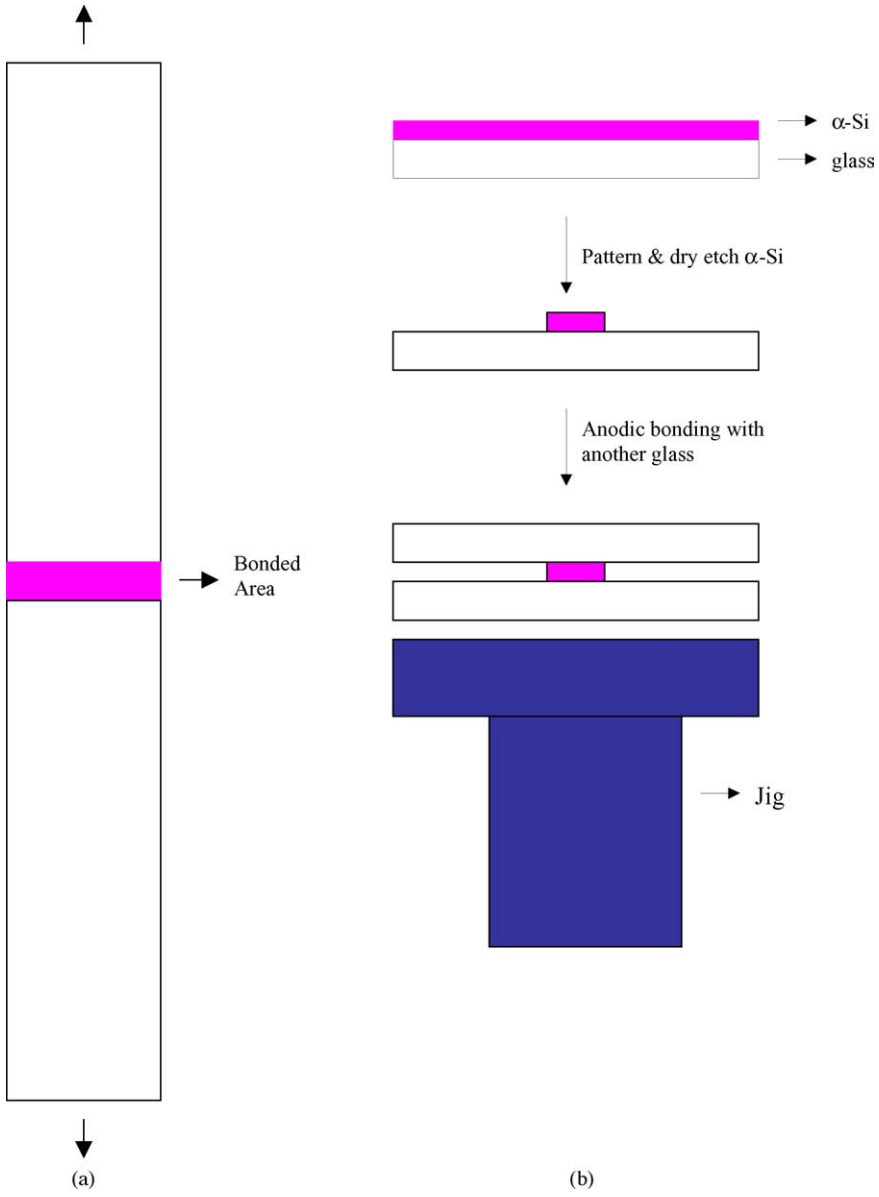

Fig. 4. Schematic of (a) 'shear' and (b) 'pull' test configuration for testing bond strength.

3. Results and discussion

3.1. Bond strength

Results of bond strength measurements carried out for a number of samples are summarized in Table 1. Pull experiments were easier to perform and most of our measurements were carried out that way. A typical experimental plot of Fig. 5 shows how a bonded sample (400 °C/3 h) fails under a pull type tensile test. The *X*-axis shows the relative displacement between two glass pieces and the *Y*-axis shows the load. The maximum load indicates the optimum force at which the

Table 1
Values of bond strength of different samples

Sample #	Material 1	Material 2	Temperature (°C)	Test type	Bond strength (N/m^2) × 10^4	Comment
1	α-Si/glass	Glass	400	Shear	111	
2	α-Si/glass	Glass	400	Pull	114	
3	α-Si/glass	Glass	400	Pull	340	Electric field applied on both sides
4	α-Si/Si_3N_4	Glass	400	Pull	110	Glass chunk remained on surface

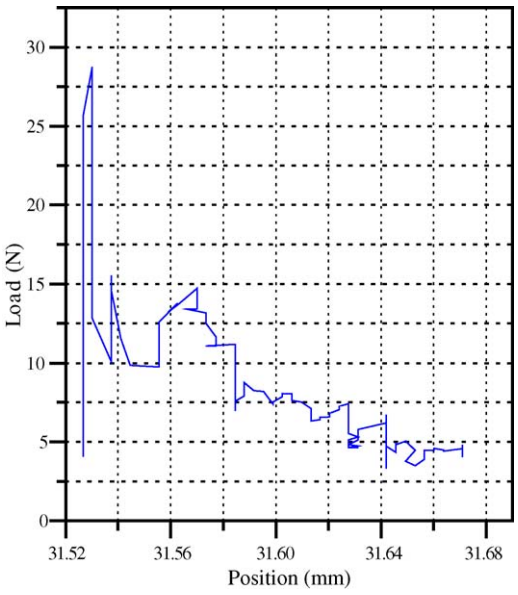

Fig. 5. Experimental plot showing bond strength for a sample (α-Si/glass, 400 °C/3 h) under pull type tensile test.

two pieces separate. In most of the initial test we observed that the α-Si layer was transferred from one glass surface to the other, indicating that the bond strength is primarily dependent on the adhesion strength of α-Si to the original glass surface. To improve adhesion of α-Si to glass, a thin silicon nitride layer was pre-deposited on glass surface, as described above. With this layer we were not able to lift α-Si from the glass. In these samples where a thin adhesion promoting silicon nitride layer is applied before α-Si deposition, two pieces of a bonded sample separate at the interface of α-Si and bare glass surface. We also attempted to reverse the electric field applied to the sample, after the bonding, in order to improve the bond between α-Si and the original glass surface on which it has been deposited. This experiment resulted in the highest bond strength of 340×10^4 N/m^2.

3.2. Nanochannel device characterization

Electrophoretic transport of ionic species in nanochannels presents unique characteristics originating from the solid–liquid interface, more precisely from the electric double-layer overlap. If the channels are in micrometer-scale, the double layer occupies a small portion of the volume and no difference between fluid behavior in these channels and in the bulk is expected. As the channels are narrowed down to the nanometer regime, the double layers starts overlapping and unique properties emerge.

A surface of the glass channel is negatively charged due to ionization of silanol groups and a positively charged diffusion layer is automatically formed near the surface. This diffusion layer, combined with the oppositely charged surface, is called electric double layer. The thickness of the diffusion layer usually varies from a few to hundreds of nanometers, depending on the solution composition [21,22]. If the dimension of a nanochannel is smaller than twice the double-layer thickness, the double layers from opposite sidewalls will overlap. When a voltage is applied across the length of the channel, we expect to see an ion depletion or accumulation in the end regions of the nanochannel [23,24]. When the nanochannel is filled with a fluorescent electrolyte (fluorescein), the ion depletion and accumulation will cause an increase and decrease in fluorescence intensity at each end of the nanochannel. In our devices, nanochannels were filled with the fluorescein solution using the reservoirs and via the U-channels. A voltage of 500 V was applied across the nanochannels and the accumulation/depletion effects were observed from all devices, demonstrating channel continuity and completeness of the seal for channel with the width of 5 μm and the length of 1 mm. Channel continuity could be obtained reproducibly for the α-Si thickness down to 50 nm.

It is interesting to note that the liquid was pulled into the nanochannel by the capillary action and no external pressure was needed. The liquid velocity was reduced with decreasing channel depth and it took about 1 min to fill the shallowest channels (50 nm deep). The electrophoretic transport experiment was performed after the solution was filled and equilibrated in all the channels for more than 5 min to ensure reproducible results.

More detailed data for 300 nm deep nanochannels, with 5 μm in width and 1 mm in length, are illustrated in Fig. 6. The connecting U-channels were filled with a solution containing 20 μM fluorescein in 100 μM sodium tetraborate (pH 9). As this solution was flushed through one U-channel, the capillary effect drew the solution into the nanochannels. After the other U-channel was flushed with the same solution, a voltage of 500 V was applied to the two U-channels with the anode in the U-channel on the left-hand side and cathode in the other U-channel. Because the U-channels were wide and deep, most of the voltage was applied across the nanochannels. A CCD camera mounted on a confocal fluorescence microscope with a 4× objective was used to monitor the fluorescence intensity change in the end regions of the nanochannels. A HBO 50 W mercury lamp was used as excitation source and a filter assembly suitable for fluorescein was used for excitation and fluorescence collection. Fig. 6 presents four consecutive images showing the fluorescence intensity change in the end regions of the nanochannels after the voltage was applied. The fluorescein in the nanochannels could not be seen because of the very small volume (1.5 pL) of fluorescein solution in the nanochannel. Before the voltage was applied, the fluorescent intensities in both U-channels were equal (Fig. 6a). Once the voltage was applied, the fluorescent intensity increased near the cathode end (right-hand side) region and decreased near the anode end (left-hand side) region of the nanochannels rapidly. The detailed interpretation of these effects in nanochannels has been described [23,24] and detailed description of the effects on different depths, channel length, electric field strength, and width with different concentrations and pH of buffer solutions will be reported elsewhere.

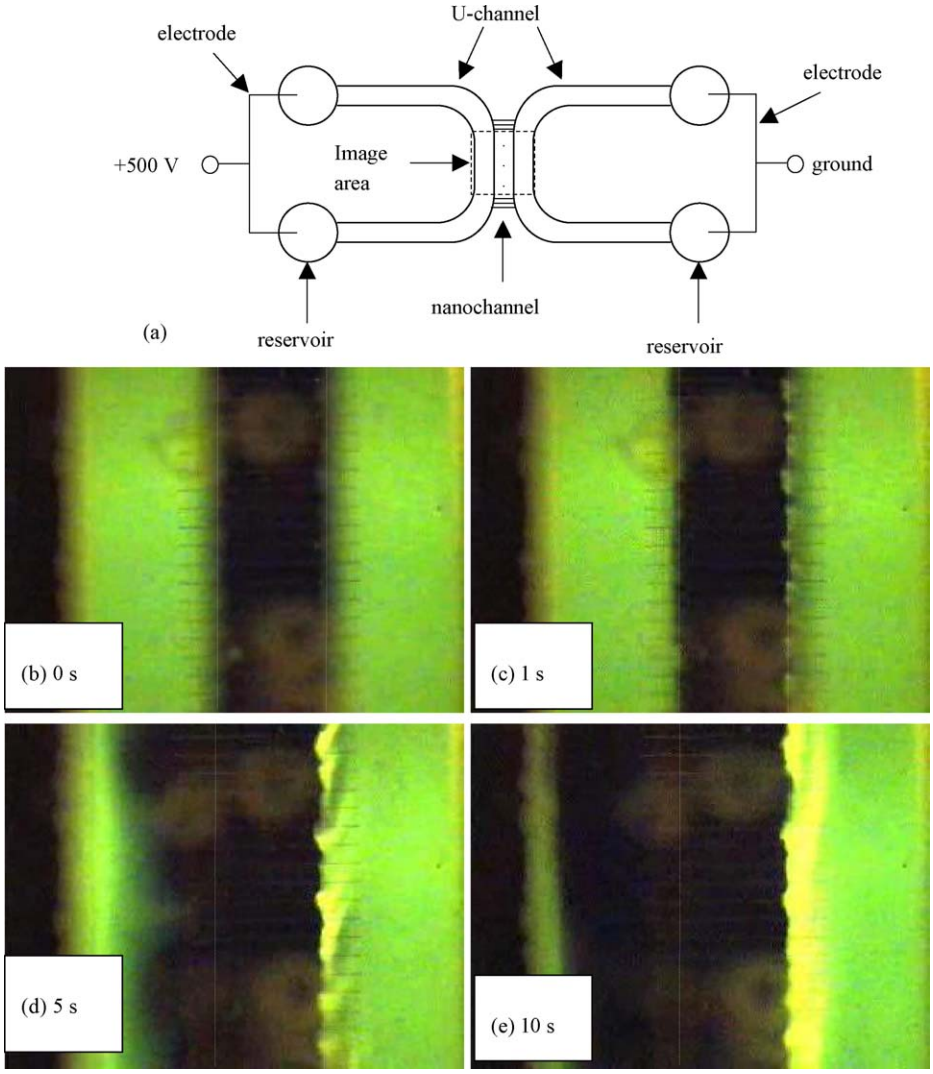

Fig. 6. Depletion/accumulation effect of nanochannels. (a) A schematic diagram of the nanochannel device. The two U-channels were connected by 50 parallel nanochannels. Nanochannel dimensions: 1 mm (L) × 5 μm (W) × 300 nm (D); U-channel dimensions: 30 mm (L) × 1 mm (W) × 50 μm (D). (b) An image from the dashed-line boxed area after 20 μM fluorescein in 100 μM sodium tetraborate (pH 9) was filled in all channels. The image was collected using a CCD camera [23,24]. (c–e) Images from the same area after a voltage of 500 V was applied across the nanochannels for 1 s, 5 s, and 10 s, respectively.

4. Conclusion

Nanochannels are realized in amorphous silicon deposited by PECVD on glass substrate. These form the basis of a nanofluidic device sealed by anodic bonding to another glass substrate. While investigating bond strength of PECVD α-Si/glass system, we found that it depends on the adhesion of α-Si to the glass substrate. An adhesion promoting layer of silicon nitride was found to improve the adhesion of α-Si to glass. A significant improvement in adhesion was also achieved by double-sided bonding resulting from the electric field reversal. The nanochannels were incorporated into a functional nanofluidic device designed to evaluate the effect of applied electric field on ion concentrations across the channel when the channel dimension becomes comparable to the thickness of the double layer.

Acknowledgements

The authors would like to thank J. Hashami and Naveen Hegde in Mechnanical Engineering of Texas Tech University for their help in tensile strength measurement and Jorge Lubguban for helping in α-Si deposition.

References

[1] H. Cao, Z. Yu, J. Wang, J.O. Tegenfeldt, R.H. Austin, E. Chen, W. Wu, S.Y. Chou, Appl. Phys. Lett. 81 (2002) 174.
[2] O. Bakajin, T.A.J. Duke, J. Tegenfeldt, C.F. Chou, S.S. Chan, R.H. Austin, E.C. Cox, Anal. Chem. 73 (2001) 6053.
[3] J.O. Tegenfeldt, O. Bakajin, C.F. Chou, S. Chan, R.H. Austin, E. Chan, T. Duke, E.C. Cox, Phys. Rev. Lett. 86 (2001) 1378.
[4] J. Han, H. Craighead, Science 288 (2000) 1026.

[5] J.O. Tegenfeldt, C. Prinz, H. Cao, S.Y. Chou, W.W. Reisner, R. Riehn, Y.M. Wang, E.C. Cox, J.C. Sturm, R.H. Austin, Proc. Natl. Acad. Sci. 101 (30) (2004) 10979.
[6] L.J. Guo, X. Cheng, C.F. Chou, Nano Lett. 4 (2004) 69.
[7] J.O. Tegenfeldt, C. Prinz, H. Cao, R.L. Huang, R.H. Austin, S.Y. Chou, E.C. Cox, J.C. Sturm, Anal. Bioanal. Chem. 378 (2004) 1678.
[8] M.B. Stern, M.W. Geis, J.E. Curtin, J. Vac. Sci. Technol. B 15 (1997) 2887.
[9] V.G. Kutchoukov, F. Laugere, W. van der Vlist, L. Pakula, Y. Garini, A. Bossche, Sens. Actuators A 114 (2004) 521.
[10] G. Wallis, D.I. Pomerantz, J. Appl. Phys. 40 (1969) 3946.
[11] J.B. Lasky, Appl. Phys. Lett. 48 (1986) 78.
[12] M. Madou, Fundamentals of Microfabrication, CRC Press, Boca Raton, 1997.
[13] T.T. Veenstra, J.W. Berenschot, J.G.E. Gardeniers, R.G.P. Sanders, M.C. Elwenspoek, A. van den Berg, J. Electrochem. Soc. 148 (2001) G68.
[14] A. Cozma, B. Puers, Micro Mechanics Europe (MME) Workshop Digest, 1994, p. 40.
[15] T. Abe, K. Sunagawa, A. Uchiyama, K. Yoshizawa, Y. Nakazato, Jpn. J. Appl. Phys. 32 (1993) 334.
[16] W.P. Maszara, G. Goetz, A. Cavigila, J.B. Mckitterick, J. Appl. Phys. 64 (1988) 4943.
[17] E. Obermeier, Electrochemical Society Proceedings, vol. 95–7, p. 212.
[18] W.B. Choi, B.K. Ju, Y.H. Lee, S.J. Jeong, N.Y. Lee, M.Y. Sung, M.H. Oha, J. Electrochem. Soc. 146 (1999) 400.
[19] A. Berthold, L. Nicola, P.M. Sarro, M.J. Vellekoop, Sens. Actuators 82 (2000) 224.
[20] J. Wei, C.K. Wong,.C. Lee, Sens. Actuators A 113 (2004) 218.
[21] A.J. Bard, L.R. Faulkner, Electrochemical Methods—Fundamentals and Applications, second ed., John Wiley & Sons Inc., 2001, pp. 546–549.
[22] R.A. Wallingford, A.G. Ewing, Capillary electrophoresis, in: Advances in Chromatography, vol. 29, 1989, pp. 1–76.
[23] S. Liu, Q. Pu, J. Yun, A. Datta, S. Gangopadhyay, H. Temkin, Emerging properties of nanochannels, in: M.A. Northrup, K.F. Jensen, D.J. Harrison (Eds.), Micro Total Analysis Systems 2003, Transducers Research Foundation Inc., 2003, pp. 657–660.
[24] Q. Pu, J. Yun, H. Temkin, S. Liu, Nano Lett. 4 (2004) 1099.